JACS
JOURNAL OF THE AMERICAN CHEMICAL SOCIETY
Article
pubs.acs.org/JACS

Benzene Selectivity in Competitive Arene Hydrogenation: Effects of Single-Site Catalyst···Acidic Oxide Surface Binding Geometry

Weixing Gu,[∇,†] Madelyn Marie Stalzer,[∇,†] Christopher P. Nicholas,[‡] Alak Bhattacharyya,[‡] Alessandro Motta,[§] James R. Gallagher,[∥] Guanghui Zhang,[∥] Jeffrey T. Miller,[∥] Takeshi Kobayashi,[⊥] Marek Pruski,[⊥,#] Massimiliano Delferro,*[,†] and Tobin J. Marks*[,†]

[†]Department of Chemistry, Northwestern University, Evanston, Illinois 60208, United States

[‡]Exploratory Catalysis Research, UOP LLC, a Honeywell Company, 25 East Algonquin Road, Des Plaines, Illinois 60017, United States

[§]Dipartimento di Chimica, Universita' degli Studi di Roma "La Sapienza" and INSTM UdR Roma, p.le A. Moro 5, I-00185, Roma, Italy

[∥]Chemical Sciences and Engineering Division, Argonne National Laboratory, Argonne, Illinois 60439 United States

[⊥]U.S. DOE Ames Laboratory, Iowa State University, Ames, Iowa 50011-3020, United States

[#]Department of Chemistry, Iowa State University, Ames, Iowa 50011-3020, United States

Supporting Information

ABSTRACT: Organozirconium complexes are chemisorbed on Brønsted acidic sulfated ZrO_2 (ZrS), sulfated Al_2O_3 (AlS), and ZrO_2–WO_3 (ZrW). Under mild conditions (25 °C, 1 atm H_2), the supported Cp*$ZrMe_3$, Cp*$ZrBz_3$, and Cp*$ZrPh_3$ catalysts are very active for benzene hydrogenation with activities declining with decreasing acidity, ZrS ≫ AlS ≈ ZrW, arguing that more Brønsted acidic oxides (those having weaker corresponding conjugate bases) yield stronger surface organometallic electrophiles and for this reason have higher benzene hydrogenation activity. Benzene selective hydrogenation, a potential approach for carcinogenic benzene removal from gasoline, is probed using benzene/toluene mixtures, and selectivities for benzene hydrogenation vary with catalyst as $ZrBz_3^+/ZrS^-$, 83% > $Cp^*ZrMe_2^+/ZrS^-$, 80% > $Cp^*ZrBz_2^+/ZrS^-$, 67% > $Cp^*ZrPh_2^+/ZrS^-$, 57%. For $Cp^*ZrBz_2^+/ZrS^-$, which displays the highest benzene hydrogenation activity with moderate selectivity in benzene/toluene mixtures. Other benzene/arene mixtures are examined, and benzene selectivities vary with arene as mesitylene, 99%, > ethylbenzene, 86% > toluene, 67%. Structural and computational studies by solid-state NMR spectroscopy, XAS, and periodic DFT methods applied to supported Cp*$ZrMe_3$ and Cp*$ZrBz_3$ indicate that larger Zr···surface distances are present in more sterically encumbered $Cp^*ZrBz_2^+/AlS^-$ vs $Cp^*ZrMe_2^+/AlS^-$. The combined XAS, solid state NMR, and DFT data argue that the bulky catalyst benzyl groups expand the "cationic" metal center–anionic sulfated oxide surface distances, and this separation/weakened ion-pairing enables the activation/insertion of more sterically encumbered arenes and influences hydrogenation rates and selectivity patterns.

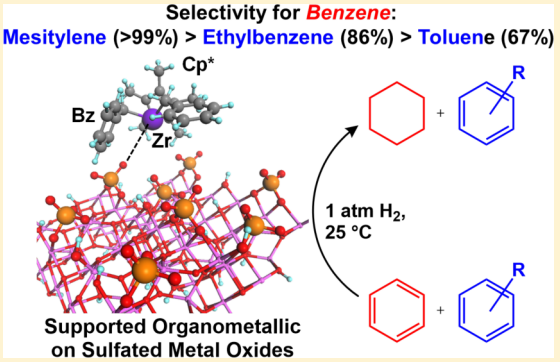

1. INTRODUCTION

Single-site supported catalysts[1] have attracted interest for both fundamental scientific and technological reasons,[2] due to the molecular level control of catalyst–substrate interactions and the selectivity that they afford. Molecular organometallic catalysts supported on Brønsted acidic sulfated oxide surfaces (Figure 1A) are especially noteworthy. The largely electrostatic interaction between the weak surface conjugate acid and the cationic metal center in such catalysts produces an electrophilic catalyst exhibiting exceptionally high activity for olefin polymerization, as well as benzene and olefin hydrogenation.[3] Moreover, 70–98% of the organometallic species chemisorbed on these surfaces are catalytically significant compared to ca. 5–10% on Lewis acidic dehydroxylated alumina (Figure 1). Additionally, chemisorption of the same precursors on surfaces with mainly weakly Brønsted acidic surface hydroxyls, such as Al_2O_3 or SiO_2, yields covalently bound, poorly electrophilic species (Figure 1C),[4−6] with unknown fractions of catalytically significant sites.[7]

This laboratory previously studied the reaction kinetics and mechanism of benzene hydrogenation mediated by Cp*$ZrMe_3$ (Cp* = $[\eta^5$-$C_5(CH_3)_5]$) adsorbed on sulfated alumina ($Cp^*ZrMe_2^+/AlS^-$) using combined ^{1}H MAS and ^{13}C

Received: December 16, 2014
Published: April 17, 2015

DOI: 10.1021/jacs.5b03254
J. Am. Chem. Soc. 2015, 137, 6770−6780

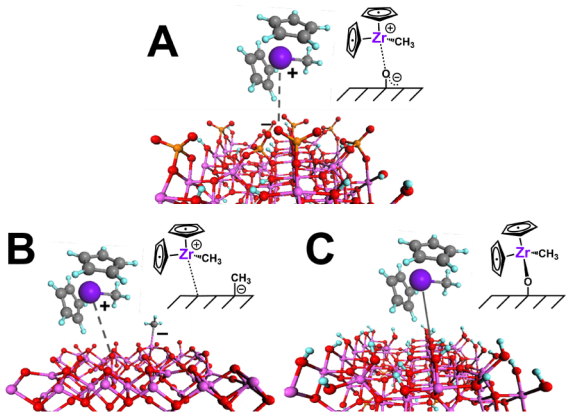

Figure 1. Proposed structures of chemisorbed Cp_2ZrMe_2 on the surfaces of highly Brønsted acidic sulfated metal oxides (A), dehydroxylated Lewis acidic metal oxides (B), and weakly Brønsted acidic hydroxylated metal oxides (C).

CPMAS NMR, EXAFS, and periodic DFT computation.[8] The data indicate formation of organozirconium cations having largely electrostatic, nondirectional $Cp^*ZrMe_2^+\cdots AlS^-$ ion-pairing with significantly elongated $Zr\cdots O_{AlS}$ distances (~2.35 Å) vs typical covalent molecular Zr(IV)-OR bonds (1.94–2.01 Å).[9] The catalytic pathway is understandable from the NMR results and DFT calculations, as proceeding via turnover-limiting delivery of the first H_2 (Scheme 1). Remarkably, $Cp^*ZrMe_2^+/AlS^-$ is one of the most active arene hydrogenation catalysts yet discovered,[10−12] and by kinetic poisoning titrations, 97 ± 2% of the Zr centers are catalytically significant for benzene hydrogenation.[3d,e] The unusually high percentage of catalytically significant sites and the very nonclassical catalytic pathway raise intriguing questions about the structure of the active catalyst, influence of the support, and substrate generality (substituted arenes vs benzene). In particular, we are interested in the ability of this class of catalyst to selectively hydrogenate benzene in the presence of other arenes.

Scheme 1. Plausible Scenario for the Turnover-Limiting Benzene Hydrogenation Step and beyond Catalyzed by Supported Cp^*ZrMe_3/Sulfated Aluminum Oxide (AlS)[8]

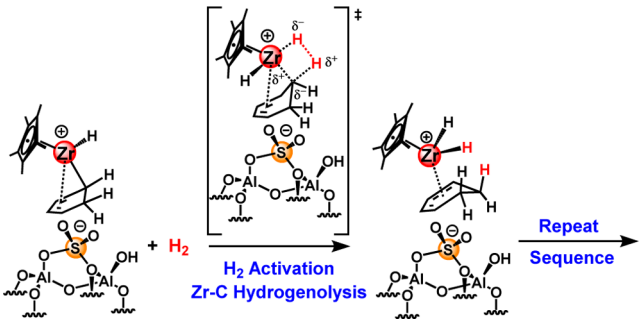

From an industrial perspective, hydrogenation of arenes presents a major challenge to catalytic science due to increasingly strict government limitations[13] on carcinogenic benzene content in gasoline.[14,15] In refineries, the most frequently utilized methods to remove benzene from the gasoline pool are:[16] (i) prefractionate the naphtha to eliminate the C_6 and/or C_7 fractions in the reformer feed;[17] (ii) extractive distillation;[18] (iii) liquid–liquid extraction;[19] (iv) zeolite-catalyzed alkylation with light olefins to form alkylbenzenes,[20−22] all of which are energy-intensive, poorly selective for benzene in the presence of other arenes, and/or produce undesired byproducts. Additionally, conventional hydrogenation catalysts such as Pd/Al_2O_3, Pt/Al_2O_3, and Ni/Al_2O_3 typically display higher selectivities for substituted arenes, which preferentially absorb on the surface and undergo subsequent hydrogenation.[23] However, these substituted arenes have high octane numbers and are desired in gasoline to compensate for the benzene removal.[24] Thus, selective benzene hydrogenation presents itself as an efficient, scalable means to remove benzene from fuels without eliminating other octane-enhancing aromatics and would represent a significant advance. Although several catalysts are known to exhibit hydrogenation activity[25] differences for neat benzene vs neat toluene,[4d,26] few studies have focused on benzene-selective hydrogenation in mixtures of aromatics.[27] Herein, we report a detailed study of competitive arene hydrogenation mediated by organozirconium complexes on a series of Brønsted acidic oxides. It will be seen that integrated solid-state NMR spectroscopy, extended X-ray absorption fine structure (EXAFS), reaction kinetic, and density functional theory (DFT) quantum chemical analysis affords unique insight into the nature of these molecule-derived surface electrophiles, leading to the discovery of new catalysts with enhanced activity and distinctive selectivity for the hydrogenation of benzene vs toluene and other arenes under mild conditions.

2. RESULTS

This contribution presents a study of the synthesis and arene hydrogenation activity of a series of organometallic catalysts chemisorbed on several strongly Brønsted acidic metal oxides. Interestingly, organozirconium catalysts are found to exhibit the highest activity and complete structural characterization is discussed for the most promising catalyst. Kinetic studies then quantify hydrogenation rates for these catalysts and identify the inhibitory effects of alkylarenes on the benzene hydrogenation. Furthermore, it will be seen that catalytic properties depend strongly on the phase of hydrogenation, as illustrated by comparing the homogeneous $Cp^*ZrMe_2^+\ X^-$ (X = $MeB(C_6F_5)_3^-$ and $B(C_6F_5)_4^-$) with heterogeneous $Cp^*ZrMe_2^+/ZrS^-$ systems.

2.1. Synthesis of Supported Organometallic Catalysts.

All organometallic catalyst precursors were prepared as described in the Experimental Section (Supporting Information). To examine the effect of the support acidity, a series of catalysts was synthesized by impregnation of Cp^*ZrMe_3, known to be a very active chemisorbed hydrogenation catalyst,[8] on sulfated alumina (AlS), sulfated zirconia (ZrS) and tungstated zirconia (ZrW). AlS, ZrS and ZrW were synthesized via literature procedures,[28,29] and the acid strengths of these materials were previously reported by the Arata group.[30] The ZrS used in this work was found to have approximately 1.24 sites/nm^2 (2.8×10^{-4} mol/g) of weak Brønsted acid sites and 1.41 sites/nm^2 (3.2×10^{-4} mol/g) of strong Brønsted acid sites. To study the effects of specific organometallic species, a series of supported catalysts was synthesized by chemisorption of Cp^*MMe_3 (M = Zr, Ti, Hf), MBz_4 (M = Zr, Ti, Hf), Cp^*TaMe_4, $(^tBuCH_2)_3Ta(CH^tBu)$, and Cp^*ZrR_3 (R = Ph, Bz) on ZrS, as this support was found produce the most active $Cp^*ZrMe_2^+$/support catalysts (Scheme 2). To quantify the amount of adsorbed metal sites, ICP-AES was utilized, except for the cases of organozirconium precatalysts on ZrS and ZrW, for which a NMR-scale test reaction of $ZrBz_4$ and the

DOI: 10.1021/jacs.5b03254
J. Am. Chem. Soc. 2015, 137, 6770−6780

Scheme 2. Synthesis of Supported Early Transition Metal Organometallic Catalysts on Sulfated Oxides

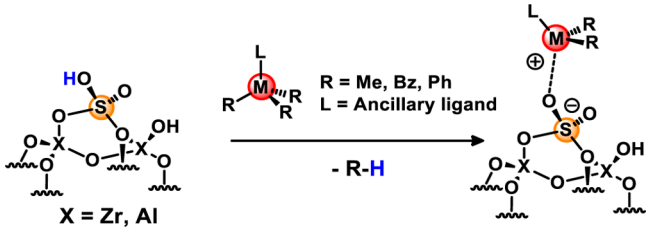

corresponding support was utilized. Using an internal standard (ethylbenzene) provides ^{1}H NMR quantification of toluene evolution, produced in a 1:1 toluene:Zr molar ratio upon chemisorption. The catalyst loadings measured were found to be solely dependent on the support, due to the susceptibility of these metal−carbon bonds to protonolysis by strong acids, and are as follows: 3.9×10^{-6} mol organometallic species/g AlS, 5.8×10^{-6} mol organometallic species/g ZrS, 4.2×10^{-6} mol organometallic species/g ZrW. These results are consistent with reports on related systems.[3,8] With these catalyst loadings, only 2% of the strong acid sites have reacted, likely due to limited reaction times and steric crowding on the surface.

2.2. Catalytic Arene Hydrogenation. Reactions were carried out in a slurry reactor with very rapid stirring (>1500 rpm) to suppress H_2 mass transfer effects (see Supporting Information for details).[8,3a,d−f] Benzene hydrogenation activity with Cp*ZrMe$_3$ on the various sulfated oxides was investigated first and the results are summarized in Table 1. Cyclohexane is

Table 1. Benzene Hydrogenation Results with Cp*ZrMe$_3$ on Various Supported Catalysts

entry	acid	highest acid strength (H_0 value)[a]	benzene hydrogenation activity (TOF)[b]
1	ZrS	−16.1	1200
2	AlS	−14.6	120
3	ZrW	−14.6	100

[a]Acid strengths of solid acids from ref 30. [b][Cp*ZrMe$_2$/MS$_x$] = 50 mg (1.95×10^{-6} mol of Zr for AlS; 2.4×10^{-6} mol of Zr for ZrS; 2.1×10^{-5} mol of Zr for ZrW), 1 h reaction time, 2 mL of benzene, 25 °C, constant 1 atm H_2, 5000 rpm. Entries performed in triplicate. TOF in (mol benzene)(mol Zr)$^{-1}$ h^{-1}.

observed as the only product for all catalysts, with no partial hydrogenation products (cyclohexene or cyclohexadiene) detected by ^{1}H NMR or GC/MS. For a given Cp*ZrMe$_3$ precatalyst, hydrogenation activity falls in the order ZrS ≫ AlS > ZrW, roughly paralleling the oxide Brønsted acidity (Table 1).[30] This agrees with previous work from our group,[3] which suggests that more acidic oxides (those having weaker conjugate bases) have weaker interactions with the cationic metal center, producing a more electrophilic organometallic surface. In marked contrast to these results, and under the same reaction conditions, the homogeneous catalysts Cp*ZrMe$_2^+$MeB(C$_6$F$_5$)$_3^-$ and Cp*ZrMe$_2^+$B(C$_6$F$_5$)$_4^-$ exhibit TOFs of only 1−2 mol benzene/mol Zr^{-1} h^{-1}, indicating that the oxide support/counteranion plays a key role in activating the surface catalytic centers. Because the heterogeneous system has an elevated number of Zr active sites (70−100%;[3e,f] determined experimentally by kinetic poisoning titration), comparable to the 100% in homogeneous systems, the difference between the heterogeneous and homogeneous systems can be associated with the creation of stronger organometallic electrophiles on the acidic support.[8] Note also that benzene hydrogenation rates are negligible with the neat sulfated oxides.

Since ZrS provides the highest hydrogenation activity, it was chosen as the support for further hydrogenation experiments. Table 2 summarizes the neat benzene and toluene hydrogenation data for the indicated organometallic precursors supported on ZrS. The organozirconium catalysts are highly active for benzene hydrogenation, and also exhibit modest activity for toluene hydrogenation. Surprisingly, the Hf, Ti, and Ta organometallics exhibit far lower activity than similar Zr complexes, even though reports showed that these organometallics supported on SiO$_2$ are competent for the hydrogenolysis of alkanes.[6q,31,32] Note, however, the Hf metallocenes are far less active polymerization catalysts than their Zr analogues.[33] The negligible activities observed in the present work could be attributed to the instability of these electrophiles on strongly acidic surfaces; however, that will be the topic of a future contribution.

Table 2. Benzene and Toluene Hydrogenation Results Over Various Supported Catalysts on ZrS[a]

entry	precursor	TOF$_{benzene}$[b]	TOF$_{toluene}$[c]
1	Cp*ZrMe$_3$	1200	2.0
2	ZrBz$_4$	450	9.8
3	Cp*ZrPh$_3$	700	110
4	Cp*ZrBz$_3$	800	340
5	Cp*ZrBz$_3$[d]	850	450
6	Cp*TiMe$_3$	7.5	0
7	TiBz$_4$	0	0
8	Cp*HfMe$_3$	0	0
9	HfBz$_4$	0	0
10	Cp*TaMe$_4$	1.9	0
11	(^{t}BuCH$_2$)$_3$Ta(CH^{t}Bu)	3.7	0

[a][Catalyst] = 50 mg (2.4×10^{-6} mol of Zr), 1 h, 25 °C, constant 1 atm H_2, 5000 rpm. Entries performed in triplicate. TOF (mol arene)(mol Zr)$^{-1}$ h^{-1}. [b]1 mL of neat benzene used as substrate. [c]1 mL of neat toluene used as substrate. [d]At 80 °C.

The organozirconium precatalysts display noteworthy activity differences for neat benzene vs pure toluene hydrogenation. Hence, they were chosen as models for investigating the hydrogenation of benzene/toluene mixtures to probe for benzene-selectivity (Table 3). Note that for Cp*ZrMe$_2^+$/ZrS$^-$ and ZrBz$_3^+$/ZrS$^-$, which exhibit exceptional benzene hydrogenation activity under neat conditions, inhibited benzene

Table 3. Competitive Arene Hydrogenation Results with the Indicated Organometallics Supported on ZrS[a]

entry	catalyst	TOF$_{benzene}$/TOF$_{toluene}$[b]	selectivity (%)[c]
1	Cp*ZrMe$_2^+$/ZrS$^-$	50/13	80
2	ZrBz$_3^+$/ZrS$^-$	50/9.8	83
3	Cp*ZrPh$_2^+$/ZrS$^-$	105/80	57
4	Cp*ZrBz$_2^+$/ZrS$^-$	500/250	67
5	Cp*ZrBz$_2^+$/ZrS$^-$[d]	550/320	63

[a][Catalyst] = 50 mg (2.4×10^{-6} mol of Zr), 1 h, 25 °C, constant 1 atm H_2, 1500 rpm. Entries performed in triplicate. TOF (mol arene)(mol Zr)$^{-1}$ h^{-1}. [b]Mixture of 1 mL of benzene + 1 mL of toluene as substrate. [c]Benzene selectivity for mixture (%) = (conversion benzene/conversion (benzene + toluene) × 100. [d]At 80 °C.

DOI: 10.1021/jacs.5b03254
J. Am. Chem. Soc. 2015, 137, 6770−6780

hydrogenation is observed in benzene/toluene mixtures (Table 3, entries 1 and 2). Additionally, in the case of $Cp^*ZrMe_2^+/ZrS^-$, toluene hydrogenation is even accelerated in the presence of benzene. In contrast, catalysts $Cp^*ZrPh_2^+/ZrS^-$ and $Cp^*ZrBz_2^+/ZrS^-$ are found to maintain high benzene hydrogenation activity, even in the presence of toluene (Table 3, entries 3 and 4).

Regarding selectivity for benzene, $ZrBz_3^+/ZrS^-$ exhibits the highest (83%) with $Cp^*ZrMe_2^+/ZrS^-$ performing similarly (80%), at comparable rates. However, $Cp^*ZrBz_2^+/ZrS^-$ exhibits a significantly greater TOF, but with somewhat lower benzene selectivity (67%) (Table 3, entries 1, 2, and 4). At 80 °C, note that $Cp^*ZrBz_2^+/ZrS^-$ exhibits increased activity for both substrates; however, reduced selectivity (63%) is also observed (Table 2 entry 5 and Table 3 entry 5).[34] Because of its high activity with retained benzene selectivity for benzene/toluene mixtures, $Cp^*ZrBz_2^+/ZrS^-$ was investigated in equimolar mixtures of benzene + other alkylarenes (Table 4).

Table 4. Benzene Hydrogenation Mediated by $Cp^*ZrBz_2^+/ZrS^-$ in the Presence of the Indicated Added Arenes and Heterocycles[a]

entry	TOF benzene	substrate[b]	TOF	selectivity (%)[c]
1	490	ethylbenzene	80	86
2	230	mesitylene	<0.1	>99
3	0.0	pyridine	0.0	–
4	0.0	thiophene	0.0	–

[a] $[Cp^*ZrBz_2^+/ZrS^-]$ = 50 mg (2.4×10^{-6} mol of Zr), 1 h, 25 °C, constant 1 atm H_2, 1500 rpm. [b] Mixture of 1 mL of benzene + 1 mL of arene as substrate. Entries performed in triplicate. TOF (mol arene)(mol Zr)$^{-1}$ h^{-1}. [c] Benzene selectivity in mixture (%) = conversion benzene/conversion (benzene + arene) × 100.

For ethylbenzene, this catalyst exhibits significant benzene selectivity (86%) and retained activity, with a benzene TOF of 490 (mol)(mol Zr)$^{-1}$ h^{-1} (Table 4 entry 1). In the presence of mesitylene, only benzene hydrogenation is observed with a TOF ~230 (mol)(mol Zr)$^{-1}$ h^{-1} and >99% selectivity. In contrast, pyridine and thiophene appear to deactivate the catalyst and $Cp^*ZrBz_2^+/ZrS^-$ displays negligible hydrogenation activity.

2.3. Arene Inhibition Effects. The aforementioned inhibition of benzene hydrogenation by the alkylated arenes was next analyzed via a simple Michaelis–Menten/Langmuir–Hinshelwood competitive inhibition model (eqs 1, 2).[35] Here

$$V_0 = \frac{d[P]}{dt} = \frac{V_{max}[S]}{K_m + [S]} \quad (1)$$

$$K_m = \frac{1 + [I]}{K_i} \quad (2)$$

V_0 is the reaction rate, $[S]$ the substrate concentration, V_{max} is the reaction rate without inhibitor present, $[I]$ is the inhibitor concentration, and K_m the Michaelis–Menten constant. K_m can then be related to the inhibitor dissociation constant, K_i, by eq 2, and is the substrate concentration at which the reaction rate = 1/2 V_{max}. Larger K_m or smaller K_i values imply larger inhibition effects. These parameters for a variety of catalysts and substrates are summarized in Table 5. Note that the K_is for the different catalysts fall in the order $Cp^*ZrBz_2^+/ZrS^-$ (1.85) > $ZrBz_3^+/ZrS^-$ (1.07×10^{-2}) > $Cp^*ZrMe_2^+/ZrS^-$ (1.58×10^{-3}). Thus, the arene hydrogenation by these supported catalysts appears to be sensitive to steric encumbrance around the metal center, with methyl group replacement by benzyl effecting a 1000× increase in K_i (Figures S1–S2). Note, however, that with the catalyst held constant, arene steric characteristics and/or electron richness of the substrate have only minor effect on the inhibition parameters.

To determine if the preferentially bound inhibitor can be removed and benzene hydrogenation activity revived, a series of four hydrogenations with the same $Cp^*ZrBz_2^+/ZrS^-$ catalyst were performed, with toluene as the substrate for the first three cycles and benzene for the fourth cycle (Figure S3A). The first three cycles reveal toluene hydrogenation proceeding as expected, while benzene hydrogenation in the fourth cycle exhibits a TOF of 760 (mol benzene)(mol Zr)$^{-1}$ h^{-1}, similar to activity of the catalyst for neat benzene (Table 2). This high fourth cycle benzene hydrogenation activity argues that any inhibitory catalyst···toluene effects do not result from permanent catalyst deactivation and are sufficiently weak to be displaced by excess benzene. Similar studies were carried out with a 1:1 benzene/toluene mixture for the first three cycles, followed by pure benzene being in the fourth (Figure S3B). The results follow a similar trend, where the fourth cycle exhibits the expected neat benzene hydrogenation activity.

2.4. Structural Characterization of the $Cp^*ZrBz_2^+/ZrS^-$ Catalyst. The structure of $Cp^*ZrBz_2^+/ZrS^-$ was investigated by a combination of solid-state NMR techniques, EXAFS, and DFT calculations. The applied NMR approaches include ^1H DPMAS, 2D $^1H-^1H$ DQMAS,[36] ^{13}C CPMAS, and 2D $^1H-^{13}C$ idHETCOR[37] NMR spectroscopy, where "DP" denotes direct polarization, "CP" $^1H-^{13}C$ cross-polarization, "MAS" magic angle spinning, "DQ" double quantum, and "idHETCOR" indirectly detected heteronuclear correlation.[38] The 1D ^1H DPMAS spectrum of $Cp^*ZrBz_2^+/ZrS^-$ measured at MAS rate ν_R = 40 kHz (Figure 2A) shows two signals centered at $\delta \approx 1.8$ and $\approx$ 6.7 ppm, assigned to aliphatic (H_{al}) and aromatic protons (H_{ar}), respectively. The single aliphatic peak results from overlap of benzyl CH_2 group and Cp* CH_3 signals, which could not be resolved (only 0.1 ppm difference is expected), even at high MAS rates.[39] The 2D $^1H-^1H$ DQMAS experiment (Figure 2B) at ν_R = 40 kHz exhibits aliphatic-aliphatic, aliphatic-aromatic, and aromatic–aromatic $^1H-^1H$ correlations. The aliphatic-aromatic correlation is shown by DFT modeling (vide infra) to result from benzylic CH_2 through-space coupling to the ortho protons of the aromatic ring (mean distance $CH_2\cdots HC_{aryl} \approx 2.50$ Å). The closest methyl protons of the Cp* are at an average distance of 4.09 Å from the benzylic aromatic protons, which is expected to be beyond the limit of the DQMAS correlation experiment. Thus, the 2D $^1H-^1H$ DQMAS spectrum is in good agreement with the proposed catalyst structure. The ^{13}C CPMAS NMR spectrum of $Cp^*ZrBz_2^+/ZrS^-$ (Figure 2C), exhibits four major resonances at δ = 128.0, 124.8, 75.2, and 11.5 ppm, with those at δ = 124.8 and 11.5 ppm straightforwardly assignable to Cp* framework and Cp*-Me carbon atoms.[3d,e,8] The signal at δ = 128.0 ppm and the downfield shifted broad signal at δ = 75.2 ppm are assigned, respectively, to the aromatic carbons and the Zr-CH_2-Ph methylene carbon. The similarity between this chemical shift and the model ion pair $Zr(CH_2Ph)_3^+B(CH_2Ph)(C_6F_5)_3^-$ (δ = 74.8 ppm)[40] compared to the covalent moiety $\{Zr(CH_2Ph)_3[(CH_3C)CO]\}$ (δ = 65.7 ppm)[41] clearly indicates

DOI: 10.1021/jacs.5b03254
J. Am. Chem. Soc. 2015, 137, 6770–6780

Table 5. Michaelis–Menten/Langmuir–Hinshelwood Parameters for the Competitive Inhibition of Benzene Hydrogenation by Various Arenes in the Presence of the Indicated ZrS-Supported Catalysts[a]

entry	inhibitor	catalyst	V_{max}	K_m	K_i
1	toluene	$Cp^*ZrMe_2^+/ZrS^-$	1200	1266	1.58×10^{-3}
2	toluene	$ZrBz_3^+/ZrS^-$	450	186	1.07×10^{-2}
3	toluene	$Cp^*ZrBz_2^+/ZrS^-$	850	1.08	1.85
4	ethylbenzene	$Cp^*ZrBz_2^+/ZrS^-$	850	1.34	1.49
5	mesitylene	$Cp^*ZrBz_2^+/ZrS^-$	850	1.66	1.20

[a][Catalyst] = 50 mg (2.4×10^{-6} mol of Zr), 1 h, 25 °C, constant 1 atm H_2, 1500 rpm. Entries performed in triplicate.

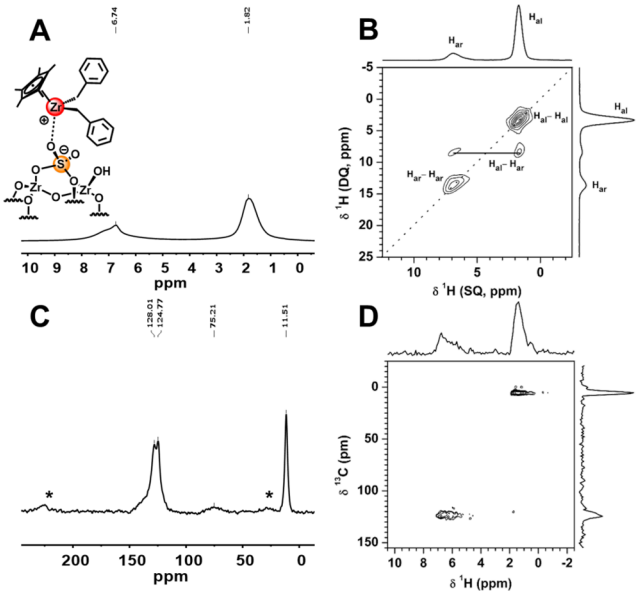

Figure 2. (A) ^1H DPMAS spectrum of $Cp^*ZrBz_2^+/ZrS^-$. The spectrum was obtained using the MAS rate ν_r = 40 kHz, the magnitude of the RF magnetic field applied to ^1H spins ν_{RF} (^1H) = 100 kHz, the recycle delay τ_{RD} = 2 s, and the number of acquisitions NS = 32. (B) $^1H-^1H$ DQMAS spectrum of $Cp^*ZrBz_2^+/ZrS^-$. The spectrum was obtained using ν_r = 40 kHz, ν_{RF} (^1H) = 100 kHz, the excitation and reconversion times = 0.1 ms, 160 rows in t_1 with Δt_1 = 25 μs and 16 scans per row, τ_{RD} = 2 s, and the total acquisition time AT = 2.8 h. (C) ^{13}C CPMAS NMR spectrum of $Cp^*ZrBz_2^+/ZrS^-$. The spectrum was obtained using ν_r = 10 kHz, the CP contact time τ_{CP} = 5 ms, τ_{RD} = 5 s, and NS = 16000. Asterisks (*) denote the MAS sidebands. (D) 2D indirectly detected $^1H-^{13}C$ through-space HETCOR spectrum of $Cp^*ZrBz_2^+/ZrS^-$. The spectrum was obtained using ν_r = 40 kHz, ν_{RF}(^1H) = 100 kHz during short pulse, ν_{RF}(^1H) = 50 kHz during CP, ν_{RF} (^1H) = 20 kHz during rotary resonance recoupling period (τ_{RR}), ν_{RF} (^1H) = 10 kHz during SPINAL64 decoupling, ν_{RF}(^{13}C) = 90 kHz during CP, ν_{RF} (^{13}C) = 10 kHz during SPINAL64 decoupling, τ_{CP} = 0.2 ms, τ_{RR} = 40 ms, 64 rows in t_1 with Δt_1 = 25 μs and 720 scans per row, τ_{RD} = 1.5 s, and AT = 38.5 h.

the formation of a "cation-like" electron-deficient organozirconium species on the surface.[3]

The $^1H-^{13}C$ idHETCOR spectrum (Figure 2D) collected with a contact time for $^1H-^{13}C$ and $^{13}C-^1H$ transfers of 0.2 ms[42] exhibits the expected aromatic and CH_3 cross-peaks, but lacks evidence of the CH_2 correlations after ~38 h of acquisition. This result is not completely unexpected, given the broadness of CH_2 resonance in the ^{13}C CPMAS spectrum, possibly due to inhomogeneity and multiple conformations on the surface.

Additional information on the catalyst structure was obtained via X-ray absorption spectroscopy (Table 6). The XANES Zr K-edge energy, 18.0000 ± 0.0003 keV, determined from the inflection point of the leading edge, is the same for $ZrBz_4$, Cp^*ZrBz_3, and the Cp^*ZrBz_2/sulfated alumina (AlS) catalyst, indicating a Zr(IV) oxidation state for all samples (Figure S4).[43] Fitting the EXAFS spectrum of the $Cp^*ZrBz_2^+/AlS^-$ catalyst was achieved via a difference method utilizing reference compounds to determine the individual ligand scattering contributions. The methodology is described in detail in the Supporting Information. This technique assumes there is little change in the bond distances and coordination geometries of the ligands in the different compounds vs the corresponding supported catalysts. Subtraction of one Zr-Cp* contribution and two Zr–Bz contributions from the supported catalyst left a residual signal due to the $Zr-O_{support}$ bonds, which was fit by 2 $Zr-O_{support}$ bonds at 2.24 Å (Table 6, Figure S5). Other models with different numbers of Zr–Bz and $Zr-O_{support}$ bonds do not fit the EXAFS data, and thus the coordination geometry of the supported catalyst is 1 Cp* (5 Zr–C at 2.47 Å), 2 Zr–Bz (2 Zr–C at 2.31 Å), and 2 $Zr-O_{support}$ bonds.

Catalyst–surface interactions were next modeled using a DFT approach, in order to relate the geometry of the chemisorbed Zr center to other structural characterization techniques. Representative complex Cp^*ZrBz_3 is analyzed on the (110) surface of sulfated alumina (Figure 3; for Cp^*ZrMe_3 see Figure S19). AlS is used here for calculations to compare with previous work[8] in which a ZrS model[44] was employed. Importantly, no significant energetic differences are found between the two. Note that there are also great similarities in adsorbed organozirconium catalyst NMR and catalytic parameters for AlS vs ZrS supports.[3e,f,8] On the basis of the computed AlS surface, two anchoring surface sites, S_A or S_B, are present which give rise to two possible Zr center–surface binding configurations. The organozirconium cation can bind between the S_A and S_B sites (Figure 3A) or at the S_B site alone (Figure 3B). The distance between the chemisorbed species and the surface is evaluated as the mean of the $Zr-O_{support}$ distances measured at all the investigated configurations, giving a distance of 2.36 Å for $Cp^*ZrBz_2^+/AlS^-$. This Zr···O distance for $Cp^*ZrBz_2^+/AlS^-$ is in good agreement with the EXAFS data (vide supra) and indicates very weak ion pairing compared to typical covalent molecular Zr(IV)-OR bonds (1.94–2.01 Å). Note also that compared to previous findings for Cp^*ZrMe_2/AlS,[8] with Zr···O = 2.32 Å, the slight Zr···O elongation here can be ascribed to the greater steric demands of benzyl versus methyl groups.

2.5. Structural Characterization of $Cp^*ZrBz_2^+/ZrS^-$ after Benzene Hydrogenation. After exposure to reaction conditions (benzene, 1 atm H_2) for 1 h, the NMR signals associated with the Zr-benzyl groups remain, but there is evidence for the formation of a catalytically active cationic $Cp^*Zr(H)Bz(\eta^n\text{-benzene})^+$ species. The partial hydrogenolysis of the benzyl ligands is supported by solid-state ^1H DPMAS, 2D $^1H-^1H$ DQMAS, ^{13}C CPMAS, and 2D $^1H-^{13}C$

DOI: 10.1021/jacs.5b03254
J. Am. Chem. Soc. 2015, 137, 6770–6780

Table 6. Fit Results Zr k-edge XANES and EXAFS (k^2: Δk = 2.7−11.6 Å^{-1}; ΔR = 1.3−2.2 Å)[a]

sample	XANES energy, keV	scatter	N	R, Å	$\Delta\sigma^2$ ($\times 10^3$)	ΔE_0, eV	comments
Zr foil	17.9980						XANES calibration
ZrO_2	18.0012						XANES reference
$Zr(acac)_4$	18.0020						XANES reference
$Zr(Bz)_4$	17.9999	$Zr-C_{Bz}$	3.9	2.29	0.0	1.1	ref 41
Cp_2ZrH_2	18.0010	$Zr-C_{Cp}$	10.1	2.51	0.0	−0.5	ref 42
Cp^*ZrBz_3	17.9997	$Zr-C_{Bz}$	2.9	2.31	2.0	−2.6	sample − Cp*
		$Zr-C_{Cp^*}$	5.3	2.47	2.0	0.3	sample − 3 Bz
$Cp^*ZrBz_2^+/AlS^-$	18.0002	$Zr-O_{support}$	1.9	2.24	2.0	−2.0	sample − 2 Bz − Cp*
$Cp^*ZrBz_2^+/AlS^-$ + benzene	18.0004	$Zr-C_{benzene}$	no difference in XANES or EXAFS compared to the catalyst in He				
		$Zr-O_{support}$	2.1	2.26	2.0	2.8	sample − 2 Bz − Cp*
$Cp^*ZrBz_2^+/AlS^-$ after hydrogenation	18.0008	$Zr-C_{aromatic}$	5.9	2.28	5.0	1.7	sample − 1 Bz − Cp*

[a] N = coordination number; R = bond distance; $\Delta\sigma^2$ = mean-square disorder in the distribution of interatomic distances; ΔE_0 = energy offset.

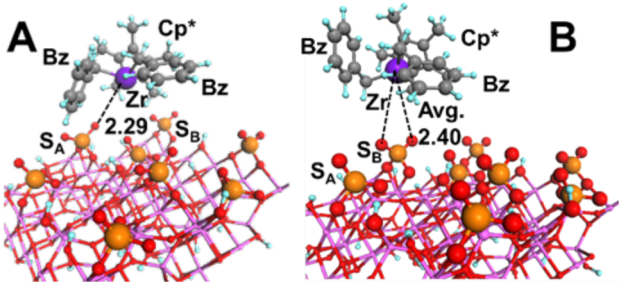

Figure 3. Energy-minimized computed chemisorbed $Cp^*ZrBz_2^+$ catalyst structures on sulfated alumina surface between site S_A (A) and S_B (B). Zr in dark violet, S in orange, O in red, H in light blue, C in gray, Al in pink.

idHETCOR[37] NMR spectroscopy, FTIR, and XAS data. The ^{1}H MAS NMR exhibits a downfield shifted broad resonance at $\delta \approx 7.4$ ppm consistent with benzene coordination to a cation-like d^0 species and an unreacted Zr-CH_2-*Ph* group (Figure S15A),[45] a broad peak at $\delta \approx 1.8$ ppm is assigned to methyl groups of the Cp* ligand and a Zr-benzyl moiety methylene group. In addition, signals at $\delta = 1.5$ ppm and $\delta = 0.9$ ppm are consistent with cyclohexane, likely physisorbed on the ZrS surface,[8] and surface OH, respectively (Figure S15A). These assignments are in agreement with 2D ^{1}H−^{1}H DQMAS and ^{1}H−^{13}C idHETCOR[37] NMR spectra, which exhibit aliphatic-aliphatic, aliphatic-aromatic, and aromatic−aromatic ^{1}H correlations, as well as ^{1H}-^{13}C cross-peaks representing aromatic and CH_3 groups (Figures S15C and S15D). Note that physisorbed cyclohexane and isolated surface OH groups are not expected to produce any detectable double-quantum ^{1}H−^{1}H coherences. The coordination of a benzene molecule to the Zr center is also evident in the ^{13}C NMR data (Figure S15B),[46] where a downfield shifted signal at $\delta = 136.4$ ppm is observed,[40,45b,47] along with a signal at $\delta = 28.5$ ppm assignable to cyclohexane molecules. The Zr−H resonance could be not identified in ^{1}H MAS NMR spectrum at room temperature, likely due to overlap with the aromatic peak centered at $\delta = 7.4$ ppm.[48] Note that the corresponding homogeneous cationic zirconocene hydride polymerization catalyst $Cp^*_2ZrH^+MeB(C_6F_5)_3^-$ exhibits a characteristic Zr−H signal at $\delta = 7.70$ ppm.[49] Partial benzyl ligand hydrogenolysis for $Cp^*ZrBz_2^+/ZrS^-$ is also supported by FTIR analysis (Figure S16). After treatment under hydrogenation reaction conditions, the aromatic C−H stretching peaks characteristic of the benzyl ligand at 3061 and 3020 cm^{-1} remain, although slightly diminished in intensity. The new and used catalysts exhibit no other differences in their vibrational spectra. Surprisingly, a characteristic Zr−H stretch[50,51] in the region of 1500−1700 cm^{-1} is not observed, likely because of the limited loading of organozirconium catalyst and overlap with Cp* and surface vibrational modes.

XANES/EXAFS were also utilized to elucidate the structure of the hydrogenolyzed catalyst (Table 6 and Figures S6−S8). The $Cp^*ZrBz_2^+/AlS^-$ EXAFS data after arene hydrogenation are most convincingly fit by Zr-Cp* and one Zr−Bz contributions (Figures S7−S8), and then fitting the residual EXAFS with 6 Zr−C bonds at 2.28 Å, consistent with an η^6 π-bonded benzene molecule. Attempting to fit a second Zr−Bz to the data results in a poor fit, and while Zr−H bonding cannot be observed explicitly by EXAFS, replacement of the lost benzyl ligand with a Zr−H is suggested. All efforts to include Zr···$O_{support}$ bonds in the model result in poor fits. Because direct evidence of a Zr−H species could not be obtained, DFT calculations were used to determine the likelihood of such a species. DFT modeling of the $Cp^*Zr(H)Bz^+\cdot C_6H_6/AlS^-$ energy-minimized structure indicates that the benzene molecule undergoes insertion between the Zr^+ and O^- ions and engages in η^6-coordination (Figure 4; for $Cp^*ZrH_2^+\cdot C_6H_6/AlS^-$ see Figure S20). As a consequence, the Zr center of the chemisorbed species is displaced substantially from the anionic surface and converges to a new conformation in which the cationic complex lies between the vicinal S_A and S_B sulfate groups. For $Cp^*Zr(H)Bz^+\cdot C_6H_6/AlS^-$, a significantly longer contact (Zr···O(S_B) = 4.25 Å) is observed than for the starting $Cp^*ZrBz_2^+/ZrS^-$ (Zr···O = 2.24 Å by EXAFS and 2.36 Å by

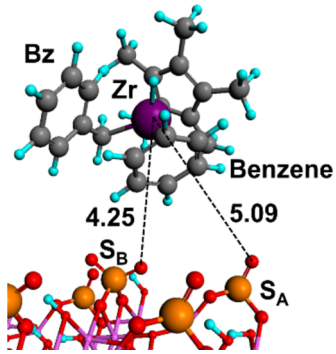

Figure 4. DFT optimized structure of $Cp^*Zr(H)Bz^+$ adsorbed on sulfated alumina. Distances are reported in Å. Zr in dark violet, S in orange, O in red, H in light blue, C in gray, Al in pink.

DOI: 10.1021/jacs.5b03254
J. Am. Chem. Soc. 2015, 137, 6770−6780

DFT). This configuration has the benzene inserted between the cationic Zr center and the S_A surface site, resulting in elongated Zr···O(S_A) distance of 5.09 Å. This computed Zr···O bond distance agrees with the EXAFS data, as such elongation results in loss of $O_{support}$ scattering signal. Thus, the agreement of the NMR, FTIR, EXAFS, and DFT data confirm the partial hydrogenolysis of the benzyl group in Cp*$ZrBz_2^+$/ZrS^-, which is seen to have a substantial impact on the arene hydrogenation activity and selectivity.

3. DISCUSSION

3.1. Supported Single-Site d^0 Catalyst Structural Effects on Arene Hydrogenation. In the present study, highly reactive "cation-like" organometallic catalysts are generated by supporting on Brønsted acidic surfaces and investigated for hydrogenation properties. At 25 °C/1 atm H_2, the organozirconium catalysts exhibit the highest activity, and activity falls with decreasing support acidity (ZrS ≫ AlS ≈ ZrW). This suggests that more acidic inorganic oxides yield stronger surface electrophiles by providing less stabilization for the "cation-like" metal center, therefore creating more reactive centers for arene hydrogenation. The catalysts $ZrBz_3^+$/ZrS^- and Cp*$ZrMe_2^+$/ZrS^- exhibit the highest selectivities for benzene hydrogenation in benzene/toluene mixtures, of 83 and 80%, respectively. However, these catalysts suffer from significant alkylarene inhibition effects, thus lowering their overall hydrogenation activity in arene mixtures. Cp*$ZrBz_2^+$/ZrS^-, while exhibiting more modest selectivity (67%) for benzene/toluene mixtures, experiences less inhibition and thus can hydrogenate mixtures containing more encumbered arenes while maintaining greater activity and selectivity (86 and >99%, respectively; Tables 4, 5). Thus, inhibition is found to be more sensitive to the catalyst structure than to that of the substrate, with multiple arenes exhibiting similar K_i values. Coordinative saturation of the catalyst then appears as the determining factor for inhibition, with less coordinatively saturated catalysts (e.g. Cp*$ZrMe_2^+$/ZrS^-) binding alkyl-substituted electron-donating substrates more strongly than coordinatively saturated catalysts (Cp*$ZrBz_2^+$/ZrS^-).

3.2. Catalyst-Surface Binding Geometry Effects on Catalytic Performance. Cp*$ZrBz_2^+$/ZrS^-, both before and after exposure to reaction conditions, was characterized in detail by NMR, EXAFS, FTIR, and DFT. The Zr···O distances found by EXAFS and DFT (2.24 and 2.36 Å, respectively) are in reasonable agreement and characteristic of weak ion pairing between the cationic metal center and the surface. This is corroborated by the catalytic results, which reveal a highly active hydrogenation catalyst. After 1 h under benzene hydrogenation reaction conditions, partial hydrogenolysis of the benzyl ligands is demonstrated, and thus Cp*Zr(H)Bz^+/ZrS^- is proposed to be the principle catalytically active species.

To better understand ligand effects on arene hydrogenation and selectivity processes, Cp*$ZrMe_2^+$/AlS^- and Cp*$ZrBz_2^+$/AlS^- hydrogenolysis were investigated by DFT. The calculations reveal that the hydrogenolysis is an exergonic process in the case of Cp*$ZrMe_2^+$/AlS^- but endergonic for Cp*$ZrBz_2^+$/AlS^- (Scheme 3). Thus, for Cp*$ZrMe_2^+$/ZrS^-, the doubly hydrogenolyzed product Cp*ZrH_2^+/ZrS^- is likely an important component of the catalytic cycle due to favorable Zr-CH_3 cleavage. In marked contrast, Zr-Bz hydrogenolysis in Cp*$ZrBz_2^+$/ZrS^- is far less favorable, possibly reflecting stronger Zr-Bz bonding,[52] and is therefore likely that partially hydrogenated Cp*Zr(H)Bz^+/ZrS^- plays a significant role in the catalytic cycle. This agrees well with the physical characterization of the spent catalyst (vide supra).

Scheme 3. Gibbs Free Energy (kcal/mol) of Zr-Alkyl Ligand Hydrogenolysis for the Cp*$ZrMe_2^+$/AlS^- and Cp*$ZrBz_2^+$/AlS^- Catalysts

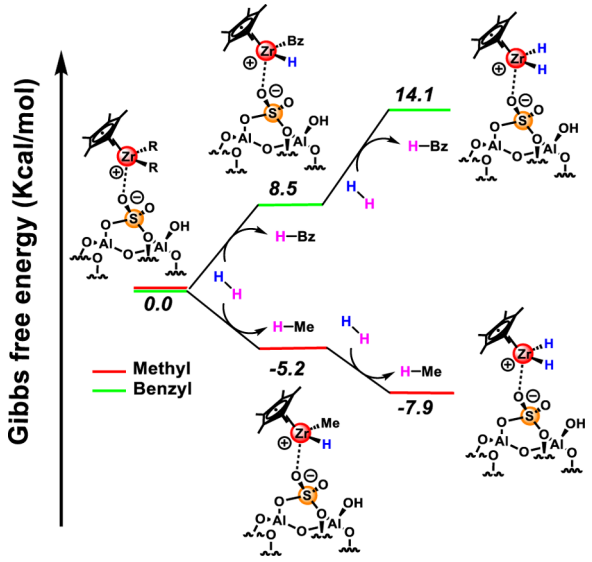

A DFT analysis was next conducted to estimate the mean distance between the Zr center of the adsorbed hydrogenated species and the sulfated oxide surface. For doubly hydrogenolyzed Cp*ZrH_2^+/AlS^-, a mean distance of ∼2.28 Å from the surface is estimated while a slightly larger distance of ∼2.38 Å is found for Cp*Zr(H)Bz^+/AlS^- (Figure 5). These distances correspond to the Gibbs free energies for heterolytically dissociating the adsorbed cations from the surface, which are computed to be ∼140 kcal/mol for Cp*ZrH_2^+/AlS^- and ∼117 kcal/mol for Cp*Zr(H)Bz^+/AlS^-. Together, these values suggest weaker ion pairing of Cp*Zr(H)Bz^+/AlS^- with the surface, likely reflecting the greater steric demands of the remaining benzyl ligand. This result is in good agreement with catalytic data (vide supra), where weaker ion pairing facilitates the activation/insertion/hydrogenation of more sterically

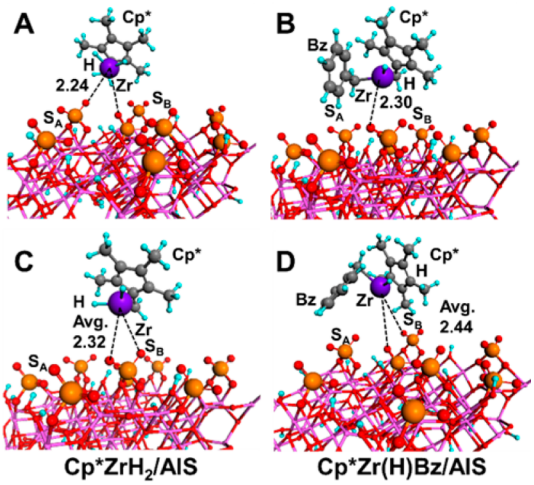

Figure 5. Optimized structures of fully hydrogenated Cp*ZrH_2^+ and partially hydrogenated Cp*Zr(H)Bz^+ adsorbed species on the sulfated alumina surface (A, B) between sites S_A and S_B; (C, D) at site S_B. Zr in dark violet, S in orange, O in red, H in light blue, C in gray, Al in pink.

DOI: 10.1021/jacs.5b03254
J. Am. Chem. Soc. 2015, 137, 6770−6780

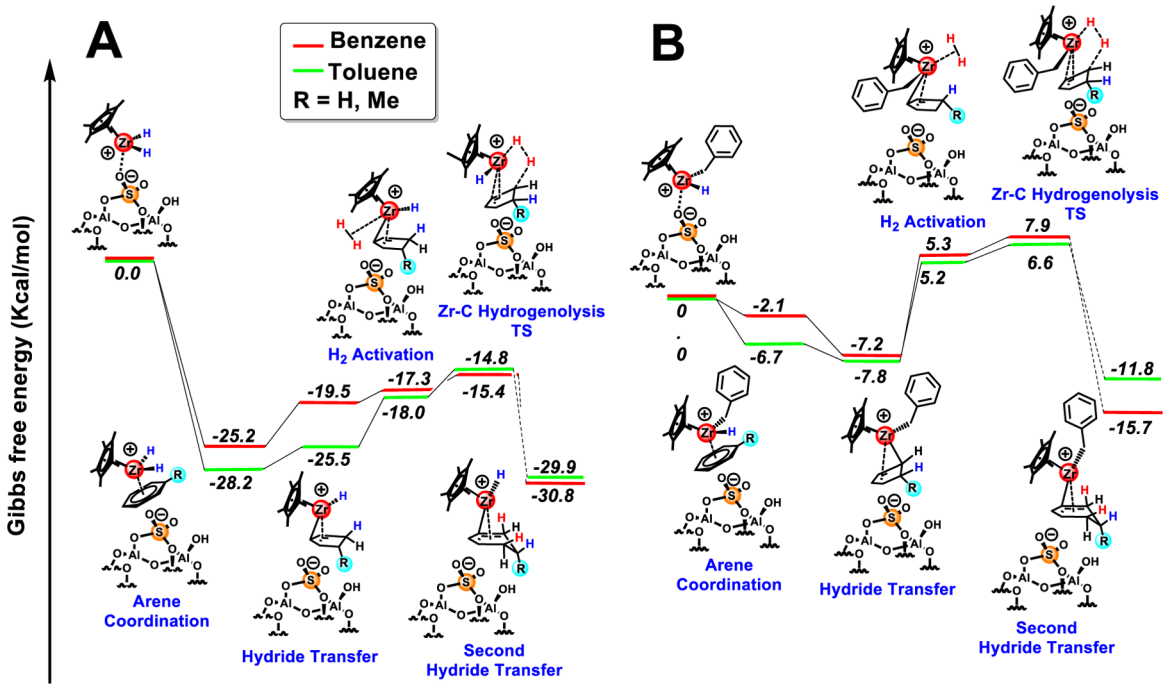

Figure 6. Gibbs free energy profile for the first subcycle of benzene and toluene hydrogenation over the indicated catalyst. (A) Cp*ZrH_2^+/AlS^-;[55] (B) Cp*Zr(H)Bz^+/AlS^-.

encumbered arenes, and thus reduces Cp*$ZrBz_2^+$/ZrS^- inhibition effects compared to Cp*$ZrMe_2^+$/ZrS^-, whose catalytic intermediate has minimal steric bulk and is more strongly bound to the surface. In sum, in this system, inhibition effects appear to be dominated by the catalyst structure rather than by that of the alkylarene inhibitor, although the latter clearly influences inhibitor TOF (Table 5).

3.3. Supported Single-Site d^0 Organometallic Catalyst Arene Hydrogenation Mechanism. DFT modeling of the toluene hydrogenation catalyzed by Cp*$ZrMe_2^+$/AlS^- was carried out and compared to the analogous process already computed for benzene (Figure S21).[8] Since partially hydrogenated arenes are not detected during the course of the hydrogenation, and the kinetics are zero-order in [benzene] and first-order for [H_2] for such systems,[3e,f] it is reasonable that the overall reaction kinetics are dominated by the first hydrogenation subcycle. Thus, the energetic comparisons focus only on the first hydrogenation subcycles computed for toluene and benzene (Figure 6). Furthermore, analysis of this first subcycle explains the distinctive catalytic properties observed experimentally. The first important note for the mechanism of Cp*ZrH_2^+/AlS^- (Figure 6A) is that toluene coordination to the electrophilic Zr center is somewhat more exoergic than is benzene ($\Delta\Delta G \approx 3.0$ kcal/mol), with the difference ascribable to the greater electron richness of toluene.[53] This greater electron donation from toluene also renders the subsequent hydride transfer from the electron-poor Zr center to be ~3.0 kcal/mol more facile for the toluene-coordinated catalyst than for the benzene analog. However, the following H_2 activation step is 5.3 kcal/mol more endergonic for toluene vs benzene due to the steric hindrance disfavoring H_2 approach. Also rendering this step endergonic for both substrates is the entropic barrier to associative H_2 approach, the slight displacement of the Zr cation from the surface required for H_2 access, and the energy required for the activation of the incoming H_2 molecule. Finally, the activation barrier of Zr–C hydrogenolysis is ~1.3 kcal/mol greater for toluene (Figure 6A). Note that in the first subcycle, Zr–C hydrogenolysis does not lead to a stable structure, but evolves directly to the first step products (hydride transfer) of the second hydrogenation subcycle, for both benzene and toluene substrates (Figure 6A). In agreement with the aforementioned experimental rate law that is zero-order in [benzene] and first-order in [H_2],[3f,8] the rate is then determined by the energetic difference between the coordinated arene species, which is the TOF determining intermediate (TDI),[54] and the Zr–C hydrogenolysis transition state, which is the TOF determining transition state (TDTS). Thus, the diminished catalytic activity for toluene hydrogenation vs benzene manifests itself in the energetic differences of these mechanistic cycles, 13.4 vs 9.8 kcal/mol, respectively. Moreover, the inhibitory effects of toluene on benzene hydrogenation can be explained by stronger stabilization of the coordinated toluene species compared with that of benzene. Thus, this mechanistic analysis for Cp*$ZrMe_2^+$/ZrS^- explains how toluene strongly competes with benzene for coordination to active sites, then turns over more slowly, inhibiting hydrogenation, in accord with experiment.

The first hydrogenation subcycle for both benzene and toluene substrates catalyzed by Cp*Zr(H)Bz^+/AlS^- is shown in Figure 6B. One significant difference between this mechanism and that of Cp*ZrH_2^+/AlS^- is the exergonic nature of arene insertion into the Zr–H bond. The stabilization for this hydride transfer step strongly increases with the steric encumbrance, thus the remaining benzyl ligand causes this step to be exergonic for both substrates. Note also that this spontaneous evolution to the hydride transfer step shifts the TDI structure from the arene coordination to the hydride transfer species, similar to the other cycle. The TDTS is again located at the Zr–C hydrogenolysis transition state (Figure 6B), which, similarly to Cp*ZrH_2^+/AlS^-, evolves directly to the first step products (hydride transfer) of the second hydrogenation subcycle for both benzene and toluene. To compare the two

DOI: 10.1021/jacs.5b03254
J. Am. Chem. Soc. 2015, 137, 6770–6780

mechanisms, the energy difference between the benzene and toluene TDI values for each catalyst was calculated, and toluene inhibition appears more efficient in $Cp^*ZrH_2^+/AlS^-$ (ΔTDI = −3.0 kcal/mol) than in $Cp^*Zr(H)Bz^+/AlS^-$ (ΔTDI = −0.6 kcal/mol), in excellent agreement with experiment (Table S1). This miniscule value for $Cp^*Zr(H)Bz^+/AlS^-$ also validates the substrate independent inhibition of this catalyst, further corroborating the experimental observations. Note that the difference in energetic barriers between toluene and benzene hydrogenation ($\Delta\Delta G$) is 3.6 kcal/mol for $Cp^*ZrH_2^+/AlS^-$, while for $Cp^*Zr(H)Bz^+/AlS^-$, $\Delta\Delta G$ < 1.0 kcal/mol (Table S1). This corresponds well with the increased benzene selectivity observed for the $Cp^*ZrMe_2^+/ZrS^-$ (80%) compared to $Cp^*ZrBz_2^+/ZrS^-$ (67%). Thus, DFT analysis provides mechanistic information well correlated with experiment as to the effects ligand tuning has on catalytic intermediates, and the resulting modifications of catalytic activity for these supported organozirconium hydrogenation catalysts.

4. CONCLUSIONS

A detailed structural/kinetic/mechanistic study of benzene hydrogenation mediated by a series of organozirconium precursors chemisorbed on various Brønsted acidic oxides was carried out. It is found that more acidic inorganic oxides yield more electrophilic and active surface catalytic species. With the same support, organozirconium complexes produce the most active hydrogenation catalysts vs related Ti, Hf or Ta based species. Although the Zr catalysts display dramatic TOF differences in the hydrogenation of neat benzene and neat toluene, toluene and other alkylarenes function as competitive inhibitors of benzene hydrogenation. Kinetic studies of inhibition by alkylarenes show that the inhibition is more sensitive to the nature of organometallic catalyst than to the substituted arene inhibitor. In hydrogenations of equimolar benzene/toluene mixtures, the selectivities for benzene hydrogenation at 25 °C vary with catalyst in the order, $ZrBz_3^+/ZrS^-$, 83% > $Cp^*ZrMe_2^+/ZrS^-$, 80% > $Cp^*ZrBz_2^+/ZrS^-$, 67% > $Cp^*ZrPh_2^+/ZrS^-$, 57%. For fixed catalyst $Cp^*ZrBz_2^+/ZrS^-$ and equimolar benzene/arene mixtures, the selectivities vary with arene in the order mesitylene (>99%) > ethylbenzene (86%) > toluene (67%). Thus, incorporation of more encumbered hydrocarbyl groups at the Zr center increases the metal-surface distance, yielding more active catalysts less susceptible to inhibition. These trends are in excellent accord with Energy-Span Analysis DFT computation.

■ ASSOCIATED CONTENT

Supporting Information

Experimental details, ^{1}H MAS NMR and ^{13}C CPMAS NMR spectra of supported catalysts, DFT calculations details, and EXAFS measurements and data analysis. The Supporting Information is available free of charge on the ACS Publications website at DOI: 10.1021/jacs.5b03254.

■ AUTHOR INFORMATION

Corresponding Authors

*m-delferro@northwestern.edu
*t-marks@northwestern.edu

Author Contributions

$^\nabla$W.G. and M.M.S. contributed equally.

Notes

The authors declare the following competing financial interest(s): Two patent applications partially based on this work have been filed (US Patent Application 14/167,603 2014 and US Patent Application 14/559,380 2014).

■ ACKNOWLEDGMENTS

Research at Northwestern University was supported by UOP, a Honeywell Company (Des Plaines, IL) and the Division of Chemical Sciences, Office of Basic Energy Sciences, Office of Energy Research, US. Department of Energy (Grant DE-FG02-86ER13511). Purchases of the NMR and GC−TOF instrumentation at the Integrated Molecular Structure Education and Research Center (IMSERC) at Northwestern U. were supported by NSF (CHE-1048773 and CHE-0923236, respectively). The CleanCat Core facility acknowledges funding from the Department of Energy (DE-FG02-03ER15457 and DE-AC02-06CH11357) used for the purchase of the Nicolet 6700 FT-IR, Harrick DRIFTS accessory, and Altamira AMI-200. Use of the Advanced Photon Source was supported by the US Department of Energy, Office of Basic Energy Sciences, under Contract DE-AC02-06CH11357. MRCAT operations are supported by the Department of Energy and the MRCAT member institutions. J.T.M., J.R.G, and G.Z.'s funding was provided by Chemical Sciences, Geosciences and Biosciences Division, US Department of Energy, under contract DE-AC0-06CH11357. Solid-state NMR studies at Ames Laboratory were supported by the U.S. Department of Energy, Office of Basic Energy Sciences, Division of Chemical Sciences, Geosciences, and Biosciences through the Ames Laboratory under Contract No. DE-AC02-07CH11358. Computational resources supporting this work were provided by the Northwestern University Quest High Performance Computing cluster (M.D.) and CINECA award N. HP10CBHAYD 2014 under the ISCRA initiative (A.M). We thank Dr. Jeffery C. Bricker of UOP for helpful discussions, J. Kotek, N. Darko, B. Lyons, and C. L. Nicholas for analytical results and helpful discussions, Dr. Jeremy Kropf for assistance with the EXAFS measurements, and Dr. N. M. Schweitzer for support on DRIFTS and TPD measurements. We also thank Albemarle Corporation (Baton Rouge, LA) for the generous gifts of tris(pentafluorophenyl) borane, $B(C_6F_5)_3$ and triphenylcarbenium tetrakis(pentafluorophenyl)-borate, $Ph_3C^+B(C_6F_5)_4^-$.

■ REFERENCES

(1) Stalzer, M. M.; Delferro, M.; Marks, T. J. *Catal. Lett.* **2015**, *145*, 3−14.

(2) (a) Wegener, S. L.; Marks, T. J.; Stair, P. C. *Acc. Chem. Res.* **2012**, *45*, 206−214. (b) Askevold, B.; Roesky, H. W.; Schneider, S. *ChemCatChem* **2012**, *4*, 307−320. (c) Rascon, F.; Wischert, R.; Coperet, C. *Chem. Sci.* **2011**, *2*, 1449−1456. (d) Sautet, P.; Delbecq, F. *Chem. Rev.* **2010**, *110*, 1788−1806. (e) Coperet, C. *Chem. Rev.* **2010**, *110*, 656−680. (f) Guzman, J.; Gates, B. C. *Dalton Trans.* **2003**, 3303−3318. (g) Copéret, C.; Chabanas, M.; Petroff Saint-Arroman, R.; Basset, J.-M. *Angew. Chem., Int. Ed.* **2003**, *42*, 156−181.

(3) (a) Williams, L. A.; Marks, T. J. *ACS Catal.* **2011**, *1*, 238−245. (b) Williams, L. A.; Marks, T. J. *Organometallics* **2009**, *28*, 2053−2061. (c) Nicholas, C. P.; Marks, T. J. *Nano Lett.* **2004**, *4*, 1557−1559. (d) Nicholas, C. P.; Marks, T. J. *Langmuir* **2004**, *20*, 9456−9462. (e) Nicholas, C. P.; Ahn, H.; Marks, T. J. *J. Am. Chem. Soc.* **2003**, *125*, 4325−4331. (f) Ahn, H.; Nicholas, C. P.; Marks, T. J. *Organometallics* **2002**, *21*, 1788−1806. (g) Ahn, H.; Marks, T. J. *J. Am. Chem. Soc.* **1998**, *120*, 13533−13534.

DOI: 10.1021/jacs.5b03254
J. Am. Chem. Soc. 2015, 137, 6770−6780

(4) (a) Joubert, J.; Delbecq, F.; Coperet, C.; Basset, J. M.; Sautet, P. *Top. Catal.* **2008**, *48*, 114−119. (b) Motta, A.; Fragala, I. L.; Marks, T. J. *J. Am. Chem. Soc.* **2008**, *130*, 16533−16546. (c) Jezequel, M.; Dufaud, V.; Ruiz-Garcia, M. J.; Carrillo-Hermosilla, F.; Neugebauer, U.; Niccolai, G. P.; Lefebvre, F.; Bayard, F.; Corker, J.; Fiddy, S.; Evans, J.; Broyer, J. P.; Malinge, J.; Basset, J.-M. *J. Am. Chem. Soc.* **2001**, *123*, 3520−3540. (d) Eisen, M. S.; Marks, T. J. *J. Mol. Catal.* **1994**, *86*, 23−50. (e) Marks, T. J. *Acc. Chem. Res.* **1992**, *25*, 57−65.

(5) (a) Tovar, T. M.; Stewart, S. M.; Scott, S. L. *Top. Catal.* **2012**, *55*, 530−537. (b) Lee, M.-Y.; Scott, S. L. *Chem.—Eur. J.* **2011**, *17*, 4632−4639. (c) Moses, A. W.; Raab, C.; Nelson, R. C.; Leifeste, H. D.; Ramsahye, N. A.; Chattopadhyay, S.; Eckert, J.; Chmelka, B. F.; Scott, S. L. *J. Am. Chem. Soc.* **2007**, *129*, 8912−8920. (d) Scott, S. L.; Church, T. L.; Nguyen, D. H.; Mader, E. A.; Moran, J. *Top. Catal.* **2005**, *34*, 109−120. (e) Ajjou, J. A. N.; Scott, S. L. *J. Am. Chem. Soc.* **2000**, *122*, 8968−8976.

(6) (a) Zhizhko, P. A.; Zhizhin, A. A.; Belyakova, O. A.; Zubavichus, Y. V.; Kolyagin, Y. G.; Zarubin, D. N.; Ustynyuk, N. A. *Organometallics* **2013**, *32*, 3611−3617. (b) Chen, Y.; Credendino, R.; Callens, E.; Atiqullah, M.; Al-Harthi, M. A.; Cavallo, L.; Basset, J.-M. *ACS Catal.* **2013**, *3*, 1360−1364. (c) Samantaray, M. K.; Alauzun, J.; Gajan, D.; Kavitake, S.; Mehdi, A.; Veyre, L.; Lelli, M.; Lesage, A.; Emsley, L.; Coperet, C.; Thieuleux, C. *J. Am. Chem. Soc.* **2013**, *135*, 3193−3199. (d) Popoff, N.; Espinas, J.; Pelletier, J.; Szeto, K. C.; Thivolle-Cazat, J.; Delevoye, L.; Gauvin, R. M.; Taoufik, M. *ChemCatChem* **2013**, *5*, 1971−1977. (e) Mori, K.; Watanabe, K.; Terai, Y.; Fujiwara, Y.; Yamashita, H. *Chem.—Eur. J.* **2012**, *18*, 11371−11378. (f) Le, R. E.; Liang, Y.; Tornroos, K. W.; Nief, F.; Anwander, R. *Organometallics* **2012**, *31*, 6526−6537. (g) Chen, Y.; Callens, E.; Abou-Hamad, E.; Merle, N.; White, A. J. P.; Taoufik, M.; Coperet, C.; Le, R. E.; Basset, J.-M. *Angew. Chem., Int. Ed.* **2012**, *51*, 11886−11889. (h) Bonati, M. L. M.; Douglas, T. M.; Gaemers, S.; Guo, N. *Organometallics* **2012**, *31*, 5243−5251. (i) Szeto, K. C.; Hardou, L.; Merle, N.; Basset, J.-M.; Thivolle-Cazat, J.; Papaioannou, C.; Taoufik, M. *Catal. Sci. Technol.* **2012**, *2*, 1336−1339. (j) Solans-Monfort, X.; Chow, C.; Goure, E.; Kaya, Y.; Basset, J.-M.; Taoufik, M.; Quadrelli, E. A.; Eisenstein, O. *Inorg. Chem.* **2012**, *51*, 7237−7249. (k) Espinas, J.; Pelletier, J. D. A.; Abou-Hamad, E.; Emsley, L.; Basset, J.-M. *Organometallics* **2012**, *31*, 7610−7617. (l) Popoff, N.; Espinas, J.; Goure, E.; Boyron, O.; Le, R. E.; Basset, J.-M.; Gauvin, R. M.; de Mallmann, A.; Taoufik, M. *Macromol. Rapid Commun.* **2011**, *32*, 1921−1924. (m) Polshettiwar, V.; Thivolle-Cazat, J.; Taoufik, M.; Stoffelbach, F.; Norsic, S.; Basset, J.-M. *Angew. Chem., Int. Ed.* **2011**, *50*, 2747−2751. (n) Pelletier, J.; Espinas, J.; Vu, N.; Norsic, S.; Baudouin, A.; Delevoye, L.; Trebosc, J.; Le, R. E.; Santini, C.; Basset, J.-M.; Gauvin, R. M.; Taoufik, M. *Chem. Commun.* **2011**, *47*, 2979−2981. (o) Goure, E.; Avenier, P.; Solans-Monfort, X.; Veyre, L.; Baudouin, A.; Kaya, Y.; Taoufik, M.; Basset, J.-M.; Eisenstein, O.; Quadrelli, E. A. *New J. Chem.* **2011**, *35*, 1011−1019. (p) Legagneux, N.; Jeanneau, E.; Thomas, A.; Taoufik, M.; Baudouin, A.; de Mallmann, A.; Basset, J.-M.; Lefebvre, F. *Organometallics* **2011**, *30*, 1783−1793. (q) Tosin, G.; Delgado, M.; Baudouin, A.; Santini, C. C.; Bayard, F.; Basset, J.-M. *Organometallics* **2010**, *29*, 1312−1322. (r) Szeto, K. C.; Norsic, S.; Hardou, L.; Le, R. E.; Chakka, S.; Thivolle-Cazat, J.; Baudouin, A.; Papaioannou, C.; Basset, J. M.; Taoufik, M. *Chem. Commun.* **2010**, *46*, 3985−3987. (s) Mazoyer, E.; Merle, N.; de Mallmann, A.; Basset, J.-M.; Berrier, E.; Delevoye, L.; Paul, J.-F.; Nicholas, C. P.; Gauvin, R. M.; Taoufik, M. *Chem. Commun.* **2010**, *46*, 8944−8946. (t) Maury, O.; Lefort, L.; Vidal, V.; Thivolle-Cazat, J.; Basset, J.-M. *Organometallics* **2010**, *29*, 6612−6614.

(7) (a) Popoff, N.; Gauvin, R. M.; De Mallmann, A.; Taoufik, M. *Organometallics* **2012**, *31*, 4763−4768. (b) Millot, N.; Soignier, S.; Santini, C. C.; Baudouin, A.; Basset, J. M. *J. Am. Chem. Soc.* **2006**, *128*, 9361−9370.

(8) Williams, L. A.; Guo, N.; Motta, A.; Delferro, M.; Fragala, I. L.; Miller, J. T.; Marks, T. J. *Proc. Natl. Acad. Sci. U. S. A.* **2013**, *110*, 413−418.

(9) The average distance found in the Cambridge Crystallographic Data Centre (CCDC, May 2014) for Zr−O single bonds is 1.988 (±12).

(10) (a) Serna, P.; Gates, B. C. *Acc. Chem. Res.* **2014**, *47*, 2612−2620. (b) Jia, H.-P.; Quadrelli, E. A. *Chem. Soc. Rev.* **2014**, *43*, 547−564. (c) Conley, M. P.; Coperet, C.; Thieuleux, C. *ACS Catal.* **2014**, *4*, 1458−1469. (d) Mondloch, J. E.; Wang, Q.; Frenkel, A. I.; Finke, R. G. *J. Am. Chem. Soc.* **2010**, *132*, 9701−9714. (e) Liu, G.; Yao, M.; Wang, J.; Lu, X.; Liu, M.; Zhang, F.; Li, H. *Adv. Synth. Catal.* **2008**, *350*, 1464−1468. (f) Warad, I.; Eichele, K.; Mayer, H. A.; Lindner, E. *Inorg. Chim. Acta* **2004**, *357*, 1847−1853. (g) Raja, R.; Thomas, J. M.; Jones, M. D.; Johnson, B. F. G.; Vaughan, D. E. W. *J. Am. Chem. Soc.* **2003**, *125*, 14982−14983. (h) Giordano, R.; Serp, P.; Kalck, P.; Kihn, Y.; Schreiber, J.; Marhic, C.; Duvail, J.-L. *Eur. J. Inorg. Chem.* **2003**, 610−617.

(11) (a) Hamdemir, I. K.; Ozkar, S.; Finke, R. G. *J. Mol. Catal. A: Chem.* **2013**, *378*, 333−343. (b) Hamdemir, I. K.; Ozkar, S.; Yih, K.-H.; Mondloch, J. E.; Finke, R. G. *ACS Catal.* **2012**, *2*, 632−641. (c) Yih, K.-H.; Alley, W. M.; Finke, R. G. *Organometallics* **2011**, *30*, 5068−5070. (d) Alley, W. M.; Hamdemir, I. K.; Wang, Q.; Frenkel, A. I.; Li, L.; Yang, J. C.; Menard, L. D.; Nuzzo, R. G.; Ozkar, S.; Yih, K.-H.; Johnson, K. A.; Finke, R. G. *Langmuir* **2011**, *27*, 6279−6294. (e) Alley, W. M.; Hamdemir, I. K.; Wang, Q.; Frenkel, A. I.; Li, L.; Yang, J. C.; Menard, L. D.; Nuzzo, R. G.; Ozkar, S.; Johnson, K. A.; Finke, R. G. *Inorg. Chem.* **2010**, *49*, 8131−8147. (f) Alley, W. M.; Hamdemir, I. K.; Johnson, K. A.; Finke, R. G. *J. Mol. Catal. A: Chem.* **2010**, *315*, 1−27. (g) Alley, W. M.; Girard, C. W.; Ozkar, S.; Finke, R. G. *Inorg. Chem.* **2009**, *48*, 1114−1121.

(12) (a) Shamshoum, E. S.; Rauscher, D. J. US5739220A, 1998. (b) Koritala, S. US176235A0, 1981. (c) Cox, J. L.; Wilcox, W. A. US863765, 1980. (d) Kroll, W. R. GB1117319, 1968. (e) Kroll, W. R. US3323902, 1967.

(13) In the United States, benzene content is currently limited to an average of 0.62 vol%, while in Australia, Canada and Europe the limit is marginally higher, at 1%. See: (a) Directive 98/69/EC of the European Parliament and of the Council of 13 October 1998, Official Journal of the European Communities, 28.12.98, L350, pp 1−56. (b) EPA MSAT2 regulation, 72 FR 8428; 2/26/07. (c) Canada SOR/97−493. (d) Australian Fuel Standard (Petrol) Determination 2001 as amended by the Fuel Standard (Petrol) Amendment Determination 2008 (no. 1). (e) Prior to 1 Jan 2011, US gasoline contained an average of 0.97 vol % benzene.

(14) Harley, R. A.; Hooper, D. S.; Kean, A. J.; Kirchstetter, T. W.; Hesson, J. M.; Balberan, N. T.; Stevenson, E. D.; Kendall, G. R. *Environ. Sci. Technol.* **2006**, *40*, 5084−5088.

(15) Conventional gasoline contains no greater than 35 wt % aromatic hydrocarbons, with an average composition of 1 wt % benzene, 7 wt % toluene, 3.5 wt % ethylbenzene, 9.7 wt % xylenes, 7.7 wt % trimethylbenzenes, 2.3 wt % tetramethylbenzenes + tetrahydronaphthalene, 0.8 wt % of pentamethylbenzene, 0.8 wt % naphthalene, 0.4 wt % methylnaphthalenes, and 1.8 wt % other multisubstituted arenes. (a) Nikolaev, V. F.; Tabrisov, I. I.; Penkovsky, A. I.; Sultanova, R. B. *Fuel* **2015**, *142*, 94−101. (b) Frysinger, G. S.; Gaines, R. B.; Ledford, E. B. *J. High Resolut. Chromatogr.* **1999**, *22*, 195−200.

(16) Meister, J.; Crowe, T.; Keesom, W.; Stine, M. *Oil Gas J.* **2006**, *104*, 38−45.

(17) (a) Dinkov, R.; Stratiev, D.; Chomakov, M.; Kirilov, K. *Pet. Coal* **2008**, *50*, 56−62. (b) Peer, R. L.; Bennett, R. W.; Felch, D. E.; von Schmidt, E. *Catal. Today* **1993**, *18*, 473−486.

(18) Lee, F. M.; Gentry, J. C. *Chem. Eng. Prog.* **1997**, *93*, 56−64.

(19) Bartholomew, C. H.; Farrauto, R. J. In *Fundamentals of Industrial Catalytic Processes*, 2nd ed.; John Wiley & Sons, Inc.: Hoboken, NJ, 2006; pp 1−970.

(20) (a) Kim, W.; Kim, J.-C.; Kim, J.; Seo, Y.; Ryoo, R. *ACS Catal.* **2013**, *3*, 192−195. (b) Laredo, G. C.; Castillo, J. J.; Navarrete-Bolanos, J.; Perez-Romo, P.; Lagos, F. A. *Appl. Catal., A* **2012**, *413−414*, 140−148. (c) Sakuneka, T. M.; Nel, R. J. J.; de Klerk, A. *Ind. Eng. Chem. Res.* **2008**, *47*, 7178−7183.

(21) Hsieh, C. R.; Robinson, R. C. Process to remove benzene from refinery streams. US5210348A, 1993.

DOI: 10.1021/jacs.5b03254
J. Am. Chem. Soc. 2015, 137, 6770−6780

(22) (a) Nicholas, C. P.; Bhattacharyya, A. US8895793, 2014;. (b) Hsieh, C. R.; Robinson, R. C. US5210348A, 1993.
(23) Mashkovsky, I. S.; Baeva, G. N.; Stakheev, A. Y.; Voskoboynikov, T. V.; Barger, P. T. *Mendeleev Commun.* **2009**, *19*, 108−109.
(24) Ramadhan, O. M.; Al-Hyali, E. A. *Pet. Sci. Technol.* **1999**, *17*, 623−635.
(25) (a) Zhou, G.; Pei, Y.; Jiang, Z.; Fan, K.; Qiao, M.; Sun, B.; Zong, B. *J. Catal.* **2014**, *311*, 393−403. (b) Youngs, T. G. A.; Manyar, H.; Bowron, D. T.; Gladden, L. F.; Hardacre, C. *Chem. Sci.* **2013**, *4*, 3484−3489. (c) Bayram, E.; Finke, R. G. *ACS Catal.* **2012**, *2*, 1967−1975. (d) Tsai, K.-Y.; Wang, I.; Tsai, T.-C. *Catal. Today* **2011**, *166*, 73−78. (e) Liu, H.; Jiang, T.; Han, B.; Liang, S.; Wang, W.; Wu, T.; Yang, G. *Green Chem.* **2011**, *13*, 1106−1109. (f) Bayram, E.; Linehan, J. C.; Fulton, J. L.; Roberts, J. A. S.; Szymczak, N. K.; Smurthwaite, T. D.; Ozkar, S.; Balasubramanian, M.; Finke, R. G. *J. Am. Chem. Soc.* **2011**, *133*, 18889−18902. (g) Zahmakiran, M.; Tonbul, Y.; Ozkar, S. *J. Am. Chem. Soc.* **2010**, *132*, 6541−6549. (h) Belskaya, O. B.; Danilova, I. G.; Kazakov, M. O.; Gulyaeva, T. I.; Kibis, L. S.; Boronin, A. I.; Lavrenov, A. V.; Likholobov, V. A. *Appl. Catal., A* **2010**, *387*, 5−12. (i) Bayram, E.; Zahmakiran, M.; Ozkar, S.; Finke, R. G. *Langmuir* **2010**, *26*, 12455−12464.
(26) Keane, M. A.; Patterson, P. M. *J. Chem. Soc., Faraday Trans.* **1996**, *92*, 1413−1421.
(27) Poondi, D.; Albert Vannice, M. *J. Catal.* **1996**, *161*, 742−751.
(28) Hino, M.; Arata, K. *J. Chem. Soc., Chem. Commun.* **1988**, 1259−1260.
(29) Hollstein, E. J.; Hsu, C.; Wei, J. T. US4956519A, 1990.
(30) Arata, K. In *Preparation of Superacidic Metal Oxides and Their Catalytic Action*; Wiley-VCH Verlag GmbH & Co. KGaA: Weinheim, 2009; pp 665−704.
(31) (a) Norsic, S.; Larabi, C.; Delgado, M.; Garron, A.; de Mallmann, A.; Santini, C.; Szeto, K. C.; Basset, J.-M.; Taoufik, M. *Catal. Sci. Technol.* **2012**, *2*, 215−219. (b) Tosin, G.; Santini, C. C.; Basset, J.-M. *Top. Catal.* **2009**, *52*, 1203−1210. (c) Chabanas, M.; Vidal, V.; Copéret, C.; Thivolle-Cazat, J.; Basset, J.-M. *Angew. Chem., Int. Ed.* **2000**, *39*, 1962−1965. (d) Rosier, C.; Niccolai, G. P.; Basset, J.-M. *J. Am. Chem. Soc.* **1997**, *119*, 12408−12409.
(32) d'Ornelas, L.; Reyes, S.; Quignard, F.; Choplin, A.; Basset, J.-M. *Chem. Lett.* **1993**, *22*, 1931−1934.
(33) Chen, Y.-X.; Metz, M. V.; Li, L.; Stern, C. L.; Marks, T. J. *J. Am. Chem. Soc.* **1998**, *120*, 6287−6305.
(34) Heller, D.; Buschmann, H.; Scharf, H.-D. *Angew. Chem., Int. Ed.* **1996**, *35*, 1852−1854.
(35) Zamostny, P.; Belohlav, Z. *Appl. Catal., A* **2002**, *225*, 291−299.
(36) Chen, Y.; Abou-Hamad, E.; Hamieh, A.; Hamzaoui, B.; Emsley, L.; Basset, J.-M. *J. Am. Chem. Soc.* **2015**, *137*, 588−591.
(37) (a) Althaus, S. M.; Mao, K.; Stringer, J. A.; Kobayashi, T.; Pruski, M. *Solid State Nucl. Magn. Reson.* **2014**, *57*−*58*, 17−21. (b) Mao, K.; Kobayashi, T.; Wiench, J. W.; Chen, H.-T.; Tsai, C.-H.; Lin, V. S. Y.; Pruski, M. *J. Am. Chem. Soc.* **2010**, *132*, 12452−12457. (c) Mao, K.; Wiench, J. W.; Lin, V. S. Y.; Pruski, M. *J. Magn. Reson.* **2009**, *196*, 92−95. (d) Wiench, J. W.; Bronnimann, C. E.; Lin, V. S. Y.; Pruski, M. *J. Am. Chem. Soc.* **2007**, *129*, 12076−12077. (e) Trebosc, J.; Wiench, J. W.; Huh, S.; Lin, V. S. Y.; Pruski, M. *J. Am. Chem. Soc.* **2005**, *127*, 7587−7593.
(38) For similar structural characterization of Cp*$ZrMe_2$/MS (M = Zr, Al) see refs 3 and 8.
(39) Xu, J.; Zheng, A.; Yang, J.; Su, Y.; Wang, J.; Zeng, D.; Zhang, M.; Ye, C.; Deng, F. *J. Phys. Chem. B* **2006**, *110*, 10662−10671.
(40) Pellecchia, C.; Grassi, A.; Immirzi, A. *J. Am. Chem. Soc.* **1993**, *115*, 1160−1162.
(41) Lubben, T. V.; Wolczanski, P. T.; Van Duyne, G. D. *Organometallics* **1984**, *3*, 977−983.
(42) The contact time used in both CP transfers (0.2 ms) limited the correlations to directly bound C−H pairs.
(43) Any attempt to fit supported organozirconium catalysts on ZrS failed. The organometallic Zr signals are totally overwhelmed by the signal from the Zr support.
(44) (a) Haase, F.; Sauer, J. *J. Am. Chem. Soc.* **1998**, *120*, 13503−13512. (b) Hofmann, A.; Sauer, J. *J. Phys. Chem. B* **2004**, *108*, 14652−14662.
(45) (a) Lavanant, L.; Silvestru, A.; Faucheux, A.; Toupet, L.; Jordan, R. F.; Carpentier, J.-F. *Organometallics* **2005**, *24*, 5604−5619. (b) Zuccaccia, C.; Stahl, N. G.; Macchioni, A.; Chen, M.-C.; Roberts, J. A.; Marks, T. J. *J. Am. Chem. Soc.* **2004**, *126*, 1448−1464. (c) Bochmann, M.; Karger, G.; Jaggar, A. J. *J. Chem. Soc., Chem. Commun.* **1990**, 1038−1039.
(46) The ^{13}C chemical shift of benzene physisorbed on ZrS is assigned at δ = 120.3 ppm. Yuzawa, H.; Aoki, M.; Itoh, H.; Yoshida, H. *J. Phys. Chem. Lett.* **2011**, *2*, 1868−1873.
(47) Noor, A.; Kretschmer, W. P.; Glatz, G.; Meetsma, A.; Kempe, R. *Eur. J. Inorg. Chem.* **2008**, 5088−5098.
(48) Wolczanski, P. T.; Bercaw, J. E. *Organometallics* **1982**, *1*, 793−799.
(49) (a) Yang, X. M.; Stern, C. L.; Marks, T. J. *Angew. Chem., Int. Ed. Engl.* **1992**, *31*, 1375−1377. (b) Yang, X.; Stern, C. L.; Marks, T. J. *J. Am. Chem. Soc.* **1994**, *116*, 10015−10031.
(50) Basset, J. M.; Ugo, R. In *Surface Organometallic Chemistry*; Wiley-VCH Verlag GmbH & Co. KGaA: Weinheim, 2009.
(51) Cho, H.-G.; Cheong, B.-S. *Bull. Korean Chem. Soc.* **2009**, *30*, 479−481.
(52) (a) Rong, Y.; Al-Harbi, A.; Parkin, G. *Organometallics* **2012**, *31*, 8208−8217. (b) Chirik, P. J.; Bercaw, J. E. *Organometallics* **2005**, *24*, 5407−5423. (c) Schock, L. E.; Marks, T. J. *J. Am. Chem. Soc.* **1988**, *110*, 7701−7715.
(53) (a) Guerrero, A.; Martin, E.; Hughes, D. L.; Kaltsoyannis, N.; Bochmann, M. *Organometallics* **2006**, *25*, 3311−3313. (b) Lin, C.-Y.; Dunbar, R. C. *Organometallics* **1997**, *16*, 2691−2697.
(54) (a) Dudnik, A. S.; Weidner, V. L.; Motta, A.; Delferro, M.; Marks, T. J. *Nat. Chem.* **2014**, *6*, 1100−1107. (b) Kozuch, S.; Shaik, S. *Acc. Chem. Res.* **2010**, *44*, 101−110.
(55) The values of benzene hydrogenation are taken from ref 8.

DOI: 10.1021/jacs.5b03254
J. Am. Chem. Soc. 2015, 137, 6770−6780